CONCN: A high-resolution, integrated surface water-groundwater ParFlow modeling platform of continental China

Chen Yang[1], Zitong Jia[2], Wenjie Xu[3], Zhongwang Wei[1], Xiaolang Zhang[4], Yiguang Zou[5],

Jeffrey McDonnell[6,7,8], Laura Condon[9], Yongjiu Dai[1], Reed Maxwell[10]

[1]School of Atmospheric Sciences, Sun Yat-sen University, Zhuhai, China

[2]College of Water Sciences, Beijing Normal University, Beijing, China

[3]Institute of Geological Survey, China University of Geosciences, Wuhan, China

[4]Department of Geosciences, Florida Atlantic University, Boca Raton, USA

[5]Department of Geography, National University of Singapore, Singapore, Singapore

[6]School of Environment and Sustainability, Global Institute for Water Security, University of Saskatchewan, Saskatoon, Canada

[7]School of Geography, Earth & Environmental Sciences, University of Birmingham, Birmingham, UK

[8]North China University of Water Resources and Electric Power, Zhengzhou, China

[9]Department of Hydrology and Atmospheric Sciences, University of Arizona, Tucson, USA

[10]Department of Civil and Environmental Engineering, High Meadows Environmental Institute, Integrated GroundWater Modeling Center, Princeton University, Princeton, USA

Correspondence to:

Chen Yang (yangch329@mail.sysu.edu.cn)

Yiguang Zou (e1144054@u.nus.edu)

Reed Maxwell (reedmaxwell@princeton.edu)

Abstract. Large-scale hydrologic modeling at the national scale is an increasing important effort worldwide to tackle ecohydrologic issues induced by global water scarcity. In this study, a surface water-groundwater integrated hydrologic modeling platform was built using ParFlow, covering the entire continental China with a resolution of 30 arcsec. This model, CONCN 1.0, has a full treatment of 3D variably saturated groundwater by solving Richards' equation, along with the shallow water equation at the ground surface. The performance of CONCN 1.0 was rigorously evaluated using both global data products and observations. RSR values (the ratio of the root mean squared error to the standard deviation of observations) show satisfied performance in streamflow, yet the streamflow is lower in the Endorheic, Hai, and Liao Rivers due to uncertainties in potential recharge. RSR values also indicate satisfied performance in water table depth of the CONCN model. It is an intermediate performance compared to two global groundwater models, highlighting the uncertainties that persist in current large-scale groundwater modeling. Our modeling work is also a comprehensive evaluation of the current workflow for continental-scale hydrologic modeling using ParFlow and could be a good starting point for the modeling in other regions worldwide, even when using different modeling systems. More specifically, the vast arid and semi-arid regions in China with substantial sinks (i.e., the end points of endorheic rivers) and the large uncertainties in potential recharge pose challenges for the numerical solution and model performance, respectively. Incompatibilities between data and model, such as the mismatch of spatial resolutions between model and products and the shorter, less frequent observation records, require further refinement of the workflow to enable fast modeling. This work not only establishes the first integrated hydrologic modeling platform in China for efficient water resources management, but it will also benefit the improvement of next generation models worldwide.

1. Introduction

China has been facing a persistent water crisis due to rapid socio-economic development and population growth (Jiang, 2009), resulting in the second lowest per inhabitant water supply among all countries worldwide (Pietz, 2017). The increasing water demand in China has been further exacerbated by more frequent hydrologic extremes, such as droughts and floods, driven by climate change and human activities. Water availability in China not only affects the nation's development trajectory but also influences the global food and supply chain (Collins and Reddy, 2022). Therefore, it is pressing to develop a consistent hydrologic modeling platform at the national scale for water resources management, water quality control, and decision-making. Some work has begun in this regard. A national-scale groundwater model with a 10 km resolution based on MODFLOW has been built (Lancia et al., 2022), and nationwide natural streamflow was reconstructed using the Variable Infiltration Capacity (VIC) model with a 0.25° resolution (Miao et al., 2022). Additionally, regional groundwater models or hydrologic models with a groundwater component have been developed for focus areas, such as the North China Plain (Cao et al., 2013; Yang et al., 2020; Yang et al., 2023a), the Heihe River Basin (Hu et al., 2016; Tian et al., 2015), the Pearl River Basin (Wang et al., 2023; Yu et al., 2022), and the Jianghan Plain in the central Yangtze River (Jiang et al., 2022). These advances in China's modeling community are valuable for quantifying the fluxes, storage, and quality of streamflow and groundwater, thereby supporting the sustainable development of the country.

There is an increasing number of national and global modeling platforms worldwide for surface water, groundwater, or a combination of both. National-scale models include the US NOAA National Water Model (NWM) (Cosgrove et al., 2024), the USGS National Hydrologic Model (NHM) (Regan et al., 2019), the ParFlow (Parallel Flow) CONUS modeling platform (Maxwell et al., 2015; Yang et al., 2023b), the Canada National Water Model (Canada1Water) (Chen et al., 2020), the British Groundwater Model (BGWM) (Bianchi et al., 2024), and the national-scale models from Germany (Belleflamme et al., 2023; Hellwig et al., 2020), France (Vergnes et al., 2023), Denmark (Henriksen et al., 2003), Netherland (Delsman et al., 2023), and New Zealand (Westerhoff et al., 2018). Global models include the hydrologic model WaterGap and its groundwater component G^{3}M (Reinecke et al., 2019; Müller Schmied et al., 2021), the hydrologic model PCR-GLOBWB and its associated groundwater models (Sutanudjaja et al., 2018; Verkaik

Deleted: national-wide

85   et al., 2024; De Graaf et al., 2015; De Graaf et al., 2017; Hoch et al., 2023), and Fan's global
86   groundwater model (Fan et al., 2013; Fan et al., 2017).

87   How to build a large-scale hydrologic model that balances high-performance with the trade-
88   off between resolution and computational efficiency is a critical issue in the hydrologic modeling
89   community, especially in groundwater modeling or modeling with a full treatment of groundwater.
90   However, it remains an open question since the subsurface is largely unseen. Reinecke et al. (2020)
91   compared the performance of several popular global groundwater models in New Zealand, along
92   with the New Zealand national groundwater model (Westerhoff et al., 2018). Reinecke et al. (2020)
93   attributed the departure of simulations from observations to model resolution, but Yang et al.
94   (2023b) suggested that the model's structure and parameters also play a role. Significant progresses
95   have been achieved in community discussions regarding model parameterization, evaluation,
96   calibration, and intercomparison (Gleeson et al., 2021; Condon et al., 2021; O'neill et al., 2021;
97   Tijerina et al., 2021). Yet, building a large-scale, high-resolution hydrologic model with satisfied
98   performance remains a challenging task (Reinecke et al., 2024; Devitt et al., 2021).

99   The most recent ParFlow CONUS 2.0 (Yang et al., 2023b) surface water-groundwater
100 integrated hydrologic model demonstrates excellent performances in both streamflow and water
101 table depth when compared with substantial observations collected from the US Geological Survey
102 (USGS) and other sources. However, the feasibility of its modeling workflow in other regions in
103 the world has not yet been evaluated. Here, we use the CONUS 2.0 workflow as a starting point
104 to build the modeling platform of continental China (CONCN). China has contrasting climatic
105 conditions, including large arid and semi-arid areas in the northwest with annual potential
106 evapotranspiration up to ~1400 mm (Li et al., 2014) and extremely wet condition in southeast with
107 annual precipitation exceeding 2000 mm (Han et al., 2023). The landforms are diverse,
108 encompassing snowpacks, wetlands, deserts, and plains. The topographic relief is dramatic,
109 ranging from the world's highest mountain ranges in Tibet to the sea level in coastal plains. All
110 these factors make China a favorable testbed for the CONUS 2.0 workflow, yet they also introduce
111 new challenges in the modeling. Additionally, the US has databases of meteorology, hydrology,
112 topography, soil, and geology, along with relatively mature systems of data management and
113 sharing. In contrast, the existence and accuracy of some necessary data in China remain uncertain.
114 These differences challenge the transferability of the CONUS 2.0 workflow, necessitating
115 modifications during the CONCN modeling process. Hence, building the CONCN model is not

116 only essential for achieving national-scale consistent management of water resources but also
117 important for identifying the strengths and limitations of the workflow. This will help improve the
118 performance of next generation models at larger or global scales.

119   In the following sections, we first introduced the structure and parameters of CONCN 1.0,
120 including the construction of hydrologically consistent topography, hydrostratigraphy, and
121 potential recharge, which are the key components of the ParFlow model. We highlighted the
122 challenges in building the CONCN 1.0 model and described the strategies to overcome these
123 obstacles. We then evaluated the performances of the CONCN model in streamflow and water
124 table depth by both global data products and observations. The comparisons of CONCN model
125 with other model products are not intended to determine which model is better but rather to identify
126 the common problems faced by the modeling community. At the end of the paper, we also
127 discussed the challenges and opportunities in integrated hydrologic modeling for communities in
128 China.

129   Note that all performance evaluations in this paper are based on the RSR value which is the
130 ratio of the root mean squared error to the standard deviation of observations. In this study, we
131 expect a satisfied performance with an RSR value less than 1.0, while 0.5 is preferable (O'neill et
132 al., 2021). However, the performances defined here are only for the comparison in this study,
133 indicating the capabilities of the model relative to the benchmark we used (i.e., global products or
134 observations). RSR values for different variables in this study (i.e., drainage area, streamflow,
135 water table depth) are not comparable. RSR values are generally not comparable with those in
136 other case studies using different models. Even for the same models used in this study, different
137 observations and different simulation periods represent different benchmarks and different system
138 dynamics, respectively, so it is hard to say the same RSR value represents the same performance
139 of a model (N. Moriasi et al., 2007; Schaefli and Gupta, 2007; Knoben et al., 2019).
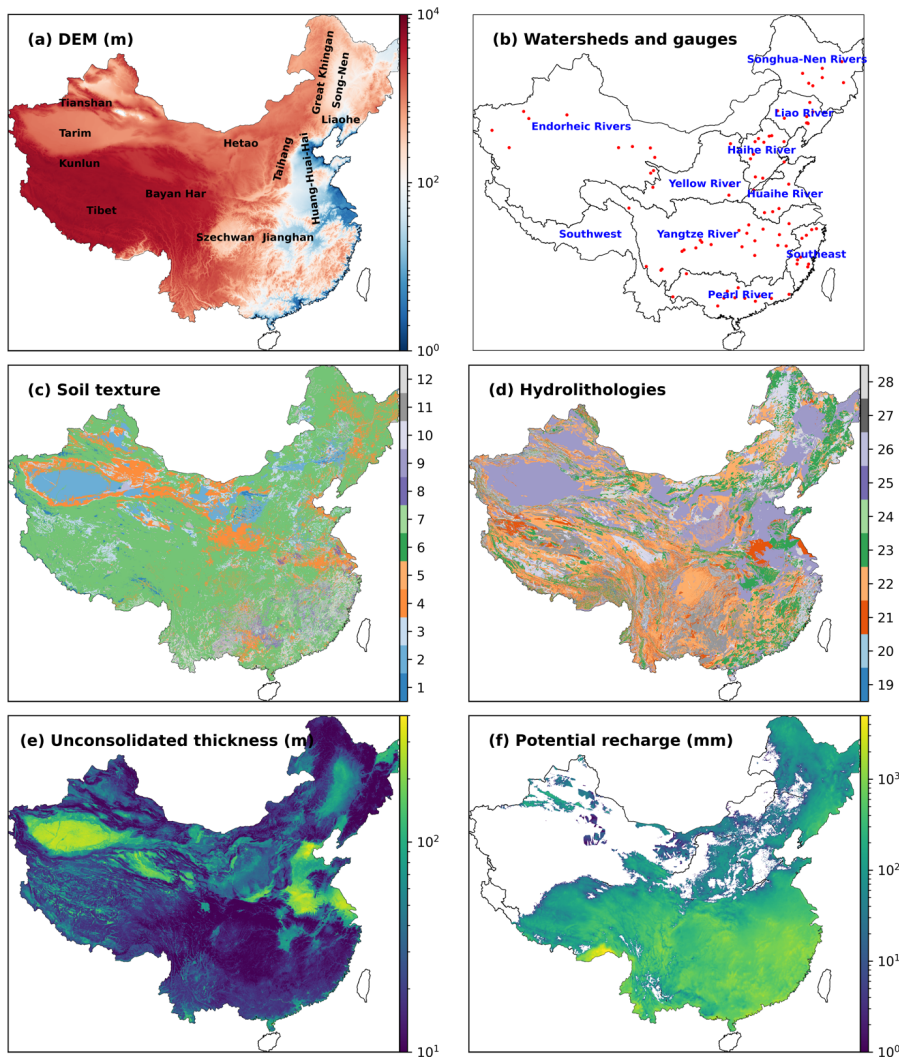
Figure 1. DEM processed by PriorityFlow and labeled with major basins, plains, and mountain ranges (a), major watersheds and streamflow gauges (red points) (b), soil texture of the top soil layer (the first layer from top to bottom) (c), hydrolithologies of the top layer (the fifth layer from top to bottom) (d), unconsolidated thickness (e), and annual potential recharge (f). The empty areas in (f) have potential recharge of zero in the model. Indicators of soil texture: 1. Sand, 2. Loamy sand, 3. Sandy loam, 4. Silt loam, 5. Silt, 6. Loam, 7. Sandy clay loam, 8. Silty clay loam, 9. Clay loam, 10. Sandy clay, 11. Silty clay, 12. Clay. **Indicators of hydrolithologies:** 19. Bedrock 1, 20. Bedrock 2, 21. f.g. sil. sedimentary, 22. sil. sedimentary, 23.

153 crystalline, 24. f.g. unconsolidated, 25. unconsolidated, 26. c.g. sil sedimentary, 27. carbonate, 28.
154 c.g. unconsolidated. f.g., sil. and c.g. represent fine-grained, siliciclastic sedimentary, and coarse-
155 grained, respectively.
156

2. Model parameterizations

158   The CONCN 1.0 model covers the entire continental China (Figure 1a) with a horizontal
159 resolution of 30 arcsec (~1 km at the equator). Vertically, the CONCN model is composed of 10
160 layers with thicknesses of 300, 100, 50, 25, 10, 5, 1, 0.6, 0.3, 0.1 m from bottom to top. This
161 structure results in 4865 and 3927 grid-cells in x and y directions, respectively, and a total of 98.8
162 million active grid-cells. Although we used the CONUS 2.0 workflow as a starting point for
163 CONCN 1.0, modifications to the workflow are necessary, as mentioned in the introduction. One
164 reason is primarily due to the data availability in China. This does not mean that the relevant data
165 is completely missing, but rather that the data is not readily available for modeling purpose, or that
166 its quality is uncertain. Another reason is due to the scientific progress that has occurred since the
167 development of the CONUS 2.0 model. For example, the total model depth of CONCN 1.0 (492
168 m) is deeper than the depth of CONUS 2.0 (392 m). The increased model depth better closes the
169 terrestrial hydrologic cycle, as groundwater contributes to global streamflow to a depth of ~500 m
170 (Ferguson et al., 2023). The details of these modifications are discussed in the following sections.

171
2.1. Topographic processing

173   The most important two components of a ParFlow model are the topographic inputs and the
174 hydrostratigraphy, which largely determine the model's performances of streamflow and
175 groundwater, respectively. Since this is a surface water-groundwater integrated hydrologic model,
176 topographic inputs may also influence the potential recharge to groundwater while
177 hydrostratigraphy is crucial for accurate simulations of baseflow. Topographic inputs refer to
178 slopes in the x and y directions, which are calculated from a digital elevation model (DEM) (Figure
179 1a). This DEM has been processed to ensure the D4 connectivity of the drainage network. D4
180 connectivity means that, within each grid-cell, streamflow is only allowed in east-west and north-
181 south directions, but not allowed in diagonal directions. The original DEM used in this study is a
182 data product with a resolution of 30 arcsec (Eilander et al., 2021), which was upscaled from the
183 MERIT Hydro DEM with a resolution of 3 arcsec (~90 m at the equator) (Yamazaki et al., 2019),

185 using an Iterative Hydrographic Upscaling approach (hereafter abbreviated as IHU DEM). The

186 IHU DEM was processed using PriorityFlow, which was developed during the CONUS 2.0

187 modeling (Condon and Maxwell, 2019). Note that the horizontal resolution of the CONCN 1.0

188 model (i.e., 30 arcsec) is set to be consistent with the resolution of this IHU DEM.

189   Reference stream networks are preferred as inputs in PriorityFlow to improve the drainage

190 performance. The challenge is that we do not have a consistent gridded stream network at the

191 national scale with a resolution close to that of CONCN 1.0, whereas a network with 250 m

192 resolution from the National Water Model (NWM) is available for CONUS 2.0 (Zhang et al., 2021).

193 As a replacement, we generated stream networks from the IHU flow direction of D8 connectivity.

194 Then we checked the generated networks with the vector networks generated from the 3 arcsec

195 MERIT Hydro flow direction (Lin et al., 2019). The initial threshold of the drainage area used to

196 generate the input networks from the IHU flow direction was set to 300 km^2. During the processing

197 using PriorityFlow, we refined some input networks locally by gradually decreasing the threshold.

198 Such refinements are necessary in areas with flat topographies (e.g., the Huang-Huai-Hai plains

199 and coastal plains in Figure 1a), where flow directions are difficult to identify without additional

200 reference networks. Endorheic rivers are common in Northern and Northwest China. Sinks, the

201 end points of these endorheic rivers, are also important to constrain flow directions and thus to

202 generate accurate D4 stream networks. Manual refinements of input networks, including the sinks,

203 were iterative processes until the networks generated by PriorityFlow appeared consistent with the

204 vector networks and there were no obvious ponding cells in runoff simulations. A total of 924 sinks

205 were identified in CONCN 1.0, compared to only 131 sinks in CONUS 2.0, which increases the

206 difficulty of the numerical solution, as ParFlow currently does not handle such water bodies.

207   In addition to the qualitative evaluation described above, we also compared the drainage areas

208 generated by PriorityFlow with those in IHU and with 294 observations collected from the

209 literature (Yin et al., 2024). Increasing performance was observed during the iterative processing

210 and the final performances are shown in Figure 2. The PriorityFlow and IHU drainage areas match

211 well, with an RSR value smaller than 1, indicating a satisfied performance (Figure 2a). An

212 additional interesting finding is the scaling relationship between drainage areas and frequencies.

213 The comparison with observations shows a much better performance, as the RSR value is smaller

214 than 0.5 (Figure 2b). Deviations from the 1:1 line were observed for drainage areas smaller than

215 100 km^2, as we focused more on drainage areas larger than 100 km^2 during the processing.

Deleted:
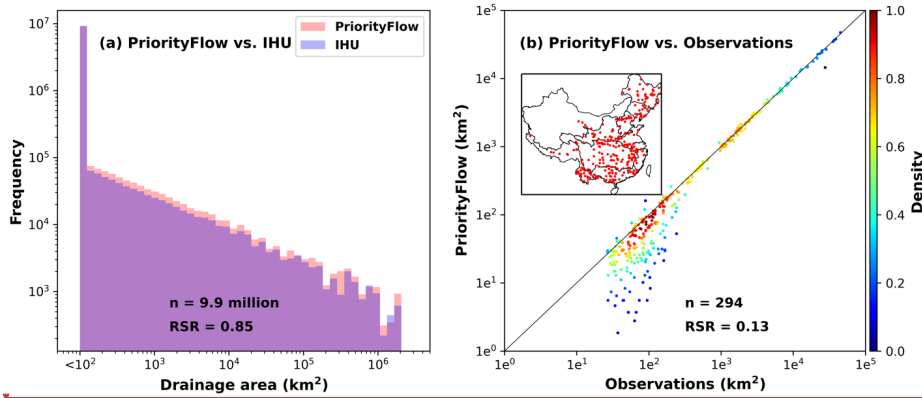
Figure 2. Evaluating the drainage performance of the topography processed by PriorityFlow using (a) IHU drainage areas and (b) observations collected from literature.

2.2. Hydrostratigraphy

The general structure of the hydrostratigraphy is composed of shallow soils and deeper hydrolithologies. The latter includes both unconsolidated and consolidated sediments (Fan et al., 2007; Huscroft et al., 2018). The details of the implementation are as follows: the top 2 m consists of four soil layers (0.1, 0.3, 0.6 and 1.0 m from top to bottom). The relative percentages of sand, clay, and silt in each layer were derived from a global dataset of soil hydraulic properties (Dai et al., 2019) with a 30 arcsec resolution. Twelve soil textures (Figure 1c) were then built from these percentages, based on the soil classification defined by the US Department of Agriculture. Hydrolithologic categories (Figure 1d) were reclassified from the permeabilities of GLHYMPS 1.0 (Gleeson et al., 2014), which was built by categorizing lithologies in the global lithology map, GLiM. GLiM was compiled by using the geologic map of 1:2.5 million scale in China area released by the China Geological Survey in 2001 (Hartmann and Moosdorf, 2012). Then *e*-folding, representing variations of hydraulic conductivity with depth and terrain slope, was applied to each of the deep six layers (Fan et al., 2007; Tijerina-Kreuzer et al., 2023). Flow barriers (Figure 1e) were implemented at the interfaces between unconsolidated and consolidated sediments via multiplying the hydraulic conductivities by 0.001 to represent a potential confining layer (De graaf et al., 2020; Huscroft et al., 2018). This concept represents the lumped effects of low-permeability sedimentary materials in the unconsolidated layer. The dataset we used to represent the interface
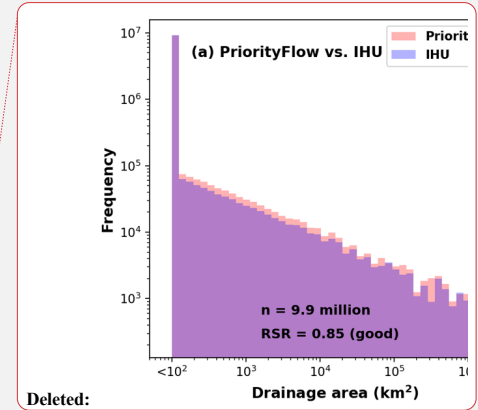
242 depths was specifically developed for China (Yan et al., 2020) and is more accurate than the global
243 version used in CONUS 2.0 (Shangguan et al., 2017).

244 We adopted this hydrostratigraphy as it is the most convincing scheme from CONUS 2.0,
245 selected through rigorous hydrologic modeling tests from hundreds of combinations of different
246 components, such as the distribution of hydrolithologic categories, anisotropy of some categories,
247 implementation of confining layers, e-folding of the hydraulic conductivities, total model depth,
248 and constant or variable depths of confining layers (i.e., flow barriers) (Swilley et al., 2023;
249 Tijerina-Kreuzer et al., 2023). The hydraulic parameters for each soil texture and hydrolithologic
250 category (e.g., hydraulic conductivity, porosity, specific yield, and parameters of the van
251 Genuchten model) were adopted from Schaap and Leij (1998) and Gleeson et al. (2014), with
252 slight calibration in the CONUS models (Maxwell et al., 2015; Yang et al., 2023b). The parameter
253 configuration assumes that each soil texture or hydrolithologic category has a set of representative,
254 scale-independent hydraulic parameters.

2.3. Potential recharge

256 The construction of potential recharge used to drive the model is the most challenging part in
257 this modeling work. Potential recharge here refers to the multi-year averaged precipitation (P)
258 minus evapotranspiration (ET), i.e., P-ET. Uncertainties of such hydrometeorological variables are
259 always high. For example, the relative standard deviation (standard deviation relative to the mean)
260 of the annual mean ET from 12 global products using different approaches reaches 50% (Jiménez
261 et al., 2011). Given this issue, the P and ET datasets selected for CONUS 2.0 were generated from
262 a VIC modeling framework (Livneh et al., 2015), which adjusts P for orographic effects and
263 ensures closure of the land surface water budget. Therefore, uncertainties of all hydrologic
264 variables were constrained within a consistent modeling system. However, datasets of P and ET in
265 China generated by various approaches have inconsistent uncertainties, and a closed water balance
266 for all hydrologic components is absent. Uncertainties in P-ET may further accumulate during data
267 processing (e.g., resampling, interpolations, and transforms) due to differences in the
268 spatiotemporal resolutions of the P and ET products and the CONCN model. Additionally, the
269 record lengths and the data quality of some datasets are hard to balance, also challenging the
270 accurate representation of a long-term average state of the predevelopment condition. We collected
271 four precipitation products and five ET products generated based on (1) interpolation of the

272   measurements (Han et al., 2023), (2) models including the Penman-Monteith equation (Running

273   et al., 2021), the complementary relationship model (Ma et al., 2019), and the land surface model

274   (Muñoz-Sabater et al., 2021), and (3) model-data fusion (Huang et al., 2014; Peng, 2020; Niu et

275   al., 2020; Zhang et al., 2019).

276   An accurate evaluation of different products was not conducted, as it is beyond the scope of

277   this study. More importantly, it will take time for the community to gradually improve the quality

278   of these datasets. We roughly evaluated the products using prior knowledge of some focus areas.

279   For example, we randomly selected several locations and compared the multi-year average levels

280   of P or ET with the commonly known levels. We used the same approach to evaluate the P-ET

281   generated by combining different P and ET datasets. For example, P-ET showed negative values

282   in some arid and semi-arid regions in northwest China where P-ET should be a dominant source

283   for known rivers. Although ERA5-Land products also provide P and ET datasets under a consistent

284   modeling framework with high enough resolution (~9 km at the equator), its precipitation dataset

285   is obviously lower than that constructed using interpolation of substantial measurements in Han et

286   al. (2023). The best combination of P (Han et al., 2023) and ET (Niu et al., 2020) in the evaluations

287   was selected to create the average state of potential recharge from 1981 to 2010 (Figure 1f).

288   However, errors induced by uncertainties from P and ET, especially ET, are still evident in some

289   regions, such as the Tarim River Basin, the Heihe River basin, and the Haihe River Basin (i.e., the

290   North China Plain). The inaccuracy estimation of potential recharge would affect the simulated

291   groundwater and streamflow as discussed in the following sections.

292   **2.4. Manning's roughness coefficients**

293   The Moderate Resolution Imaging Spectroradiometer (MODIS) Land Cover Type (MCD12Q1)

294   version 6.1 data product with a 500 m resolution (Friedl and Sulla-Menashe, 2022) was used to

295   build the distribution of Manning's roughness coefficients, which are necessary for calculating

296   streamflow, and will also be required by the Common Land Model (CLM) (Dai et al., 2003) in the

297   future transient ParFlow-CLM model (Kollet and Maxwell, 2008). The land cover types in this

298   product follow the International Geosphere-Biosphere Programme (IGBP) classification, which is

299   consistent with the classification required by ParFlow-CLM. In the modeling of CONUS 2.0, a

300   land cover map with a higher resolution of 30 m was reclassified into the IGBP classification.

301   Some products with resolutions higher than 500 m are also available in China (Yang and Huang,

302 2021), but their coarse classifications prevented us from reclassifying the types to subtypes. Stream
303 networks were generated using PriorityFlow with a threshold drainage area of 50 km^2, and stream
304 orders were calculated based on the Strahler stream order (Strahler, 1957). Manning's roughness
305 coefficients were set to vary by land cover type and were further adjusted in stream channels,
306 decreasing in value with increasing stream order. The values of Manning's roughness coefficient
307 for each land cover type and each stream order were adapted from the National Water Model
308 (Gochis et al., 2015) and a previous study (Foster et al., 2020).

3. ParFlow modeling platform

310 ParFlow simulates the movement of 3D variably saturated groundwater and 2D surface water
311 simultaneously by solving Richards' equation with the shallow water equation as the top boundary
312 (Kollet and Maxwell, 2006). CONCN 1.0 uses a terrain following grid, which significantly reduces
313 the computational load compared to an orthogonal grid (Maxwell, 2013). The model was
314 initialized with a uniform water table depth (WTD) of 2 m and was driven by the average potential
315 recharge of 1981–2010 to achieve a quasi-steady state for evaluations in following sections. All
316 faces of the model, except the top boundary, are no flow boundaries. We ran the model using the
317 seepage face boundary condition on top of the model until the total storage change was less than
318 1% of the potential recharge. This is to form the topography-driven patterns of water table.
319 Afterward, the overland kinematic boundary condition was enabled to generate river systems. The
320 spinup continued until the total storage change was less than 3% of the potential recharge. River
321 systems quickly reached a quasi-steady state in groundwater convergence areas, which had already
322 been identified in the first stage. This two-phase spinup process omitted unnecessary surface water-
323 groundwater interactions during the early stage to improve computational efficiency. Although the
324 dimension of CONCN 1.0 is comparable to CONUS 2.0, CONCN 1.0 required more time for
325 spinup because rivers in arid and semi-arid regions take longer to reach a quasi-steady state, as the
326 water is limitedly recharged by local precipitation but is sourced from the far away upstream.

327 The Newton-Krylov approach is employed to solve this large nonlinear system, which is
328 discretized on a finite difference grid in an implicit manner. Parallel scalability of the model is
329 ensured by using a multi-grid preconditioner. Thresholds of nonlinear and linear iterations are 1e^{-5}
330 and 1e^{-10}, respectively, to ensure proper convergence. The model was run on Princeton Della
331 GPU cluster using four 80-GB NVIDIA A100 GPU cards, or on the NCAR Derecho

332 supercomputer using 4096 processor cores across 32 nodes. Each node on Derecho is equipped
333 with 3rd Gen AMD EPYC™ 7763 Milan CPUs.
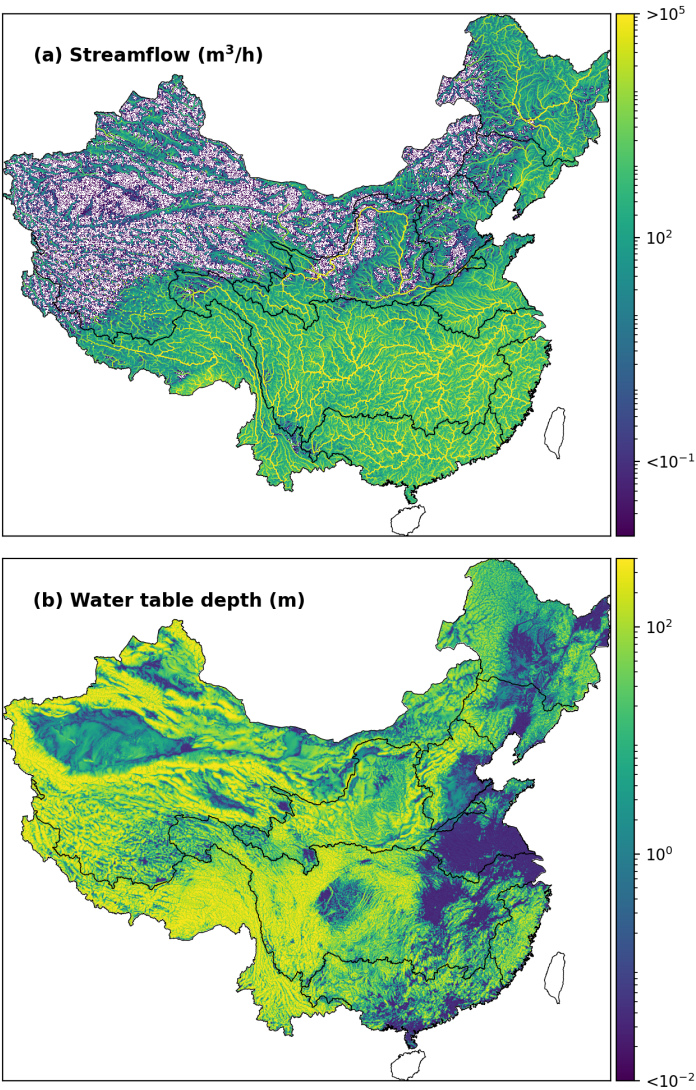
334
335 **Figure 3. Simulated streamflow and water table depth by CONCN 1.0, representing the**
336 **average state from 1981 to 2010.**

337

4. Simulations and evaluations

The simulated streamflow and WTD are shown in Figure 3. Patterns of streamflow (Figure 3a) reveal a contrast between wet and dry regions, generally consistent with the monsoon and non-monsoon regions. Large river systems in the monsoon region are well represented, such as the Yellow River in northern China, the Yangtze River and the Pearl River in southern China, and the Songhua, Nen, and Liao Rivers in northeast China. During the spinup, we observed that the Yellow River is primarily recharged by water sourced from the Bayan Har Mountain ranges and by a small amount of local groundwater. The number of river segments recharged by precipitation increases downstream the Hetao Plain. River systems in northwest China are also visible, though future work is needed to improve the accuracy by reducing uncertainties in potential recharge. The WTD (Figure 3b) presents topography-driven patterns, showing shallow water tables in the Huang-Huai-Hai Plain, the Jianghan Plain, the Liaohe Basin, and the Songnen Plain. The water table is also shallow inside the Tarim Basin, where the terrain is flat, even though annual precipitation there is lower than 50 mm. Deep water tables are distributed along the Tianshan and Kunlun Mountain ranges, the Taihang-Great Khingan Mountain ranges, and the transition area from the Tibet Plateau to the Szechwan Basin.

The performance of CONCN 1.0 was comprehensively evaluated by both data products and observations. In the evaluation using measured observations, it is difficult to ensure that the duration of the records is consistent with that of the potential recharge (1981–2010), as streamflow or groundwater observations earlier than 2000 are hard to collect. This mismatch between the simulation and observation periods may cause discrepancies between simulated and observed values, due to the different drivers resulting from interannual variations of P and ET. This highlights a new challenge relative to the CONUS 2.0 modeling, as publicly accessible observations in the US date back to 1900 or even earlier.

4.1. Evaluation of streamflow

We compared the simulations of CONCN 1.0 with a global streamflow dataset, GRADES-HydroDL (Yang et al., 2023c). The daily streamflow from 1980 to present is estimated for 2.94 million river reaches by applying a Long Short-Term Memory (LSTM) model on a 0.25° grid, developed following Feng et al. (2020), and then coupling the LSTM model with a river routing model (RAPID) (David et al., 2011). River reaches with drainage areas larger than 1000 km^2 were

368 selected, and those with drainage areas larger than 120% or smaller than 80% of the PriorityFlow

369 drainage areas were further filtered out. For each of the selected 23,609 reaches, streamflow during

370 the potential recharge period (1981 to 2010) was averaged and compared with the simulation of

371 CONCN 1.0. Locations of the selected reaches and a scatterplot of simulations vs. GRADES-

372 HydroDL are shown in Figure 4. Overall, we see comparable performances of CONCN 1.0 and

373 GRADES-HydroDL, with an RSR value close to 1. Smaller streamflow values are more scattered

374 in the plot due to the uncertainties associated with smaller drainage areas.

375

Figure 4. Scatterplot of simulated streamflow vs. GRADES-HydroDL. Locations of the selected reaches for comparison are shown in the upper left corner.

Deleted:
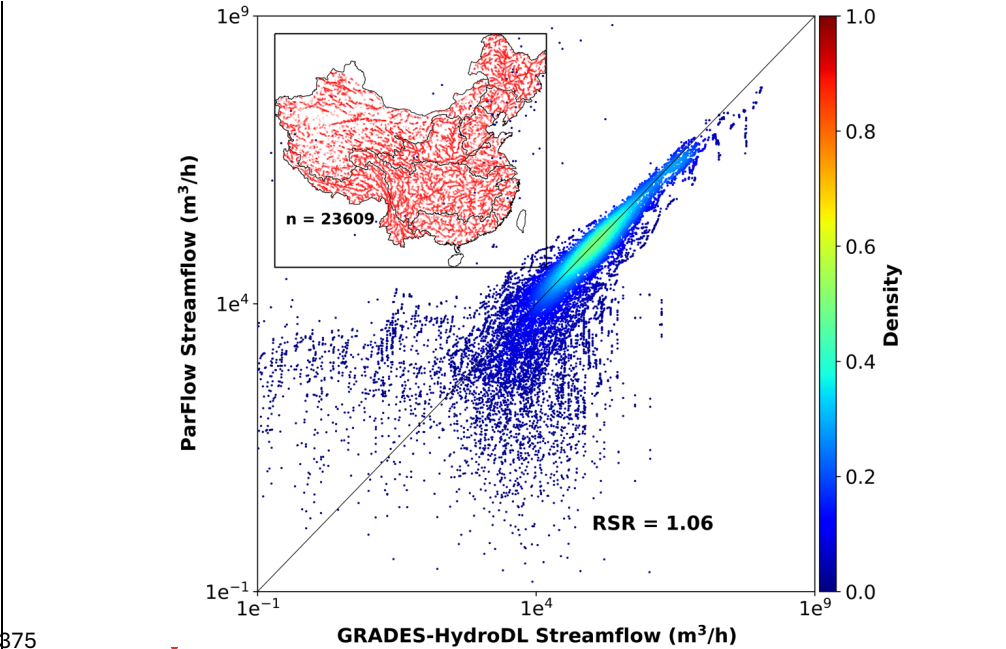
379 We collected streamflow observations at 95 gauges from the annual River Sediment Bulletin

380 of China, with 88 gauges available for evaluation. Five gauges were removed because we could

381 not find their locations (i.e., latitude and longitude) in the lookup table of national gauges, one of

382 two very close gauges was also removed, and one gauge in Hainan province was excluded as it is

383 out of the modeling domain. Locations of the 88 gauges are shown in Figure 1b, covering most of

385   the modeling domain to ensure an impartial evaluation. However, the number of gauges is
386   obviously limited, and augmenting the database for this modeling platform will take time. The
387   observations include monthly records spanning from 2002 to 2021. Although most gauges do not
388   have a complete 20-year record, each gauge has at least a two-year record. Scatterplots of
389   simulations vs. observations are shown in Figure 5. Most basins show satisfied performances, with
390   RSR values close to 1.0 or smaller than 0.5. Simulated streamflow of the Endorheic, Haihe and
391   part of the Liao Rivers is much lower than observed. This is likely due to uncertainties in potential
392   recharge, as discussed in section 2.3 and the fact that simulations at these gauges are mainly
393   baseflow sourced from groundwater. Slight deviations are also seen along the mainstream of the
394   Yangtze and Yellow Rivers, likely caused by hydraulic engineering, such as dam operations.

395
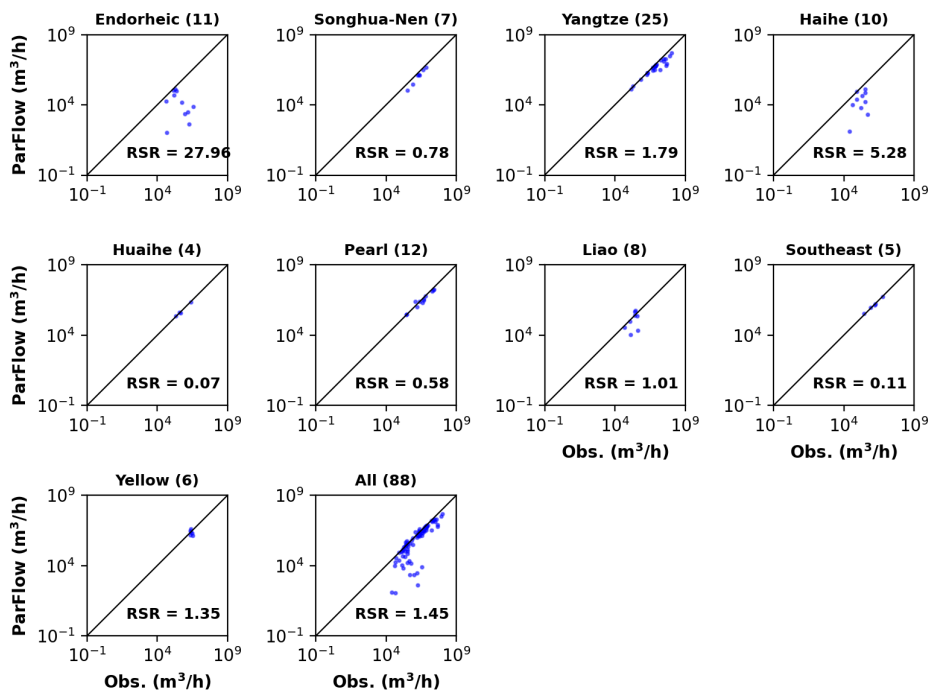
396
397   **Figure 5. Scatterplots of simulated vs. observed streamflow for basins in Figure 1b and the**
398   **entire CONCN 1.0 domain.**
399
400   **4.2. Evaluation of water table depth**

402   WTDs generated by two global groundwater models were collected (Figures 6a-b). Both

403   models have a horizontal resolution of 30 arcsec, but their formulations and vertical structures

404   differ significantly from CONCN 1.0. The first model is a horizontal, two-dimensional

405   groundwater model of 40 layers. It describes 1D soil water movement within each column using

406   Richards' equation and 2D lateral flow among columns using Darcy's law under the Dupuit-

407   Forchheimer assumption. It is an inverse modeling originally developed by Fan et al. (2017) and

408   later updated in 2020 [as eLetters in Fan et al. (2013)]. The water table in Figure 6a is the average

409   of hourly dynamics from 2004 to 2014. The second model, GLOBGM v1.0, is a three-dimensional

410   groundwater model with two layers, driven by outputs from PCR-GLOBWB (Verkaik et al., 2024).

411   GLOBGM v1.0 is a steady-state model representing the average state for the period 1958–2015.

412   It is a refined version of the 5 arcmin PCR-GLOBWB-MODFLOW model (De Graaf et al., 2015;

413   De Graaf et al., 2017). Though GLOBGM v1.0 is not calibrated, its predecessor (De Graaf et al.,

414   2017) was calibrated.
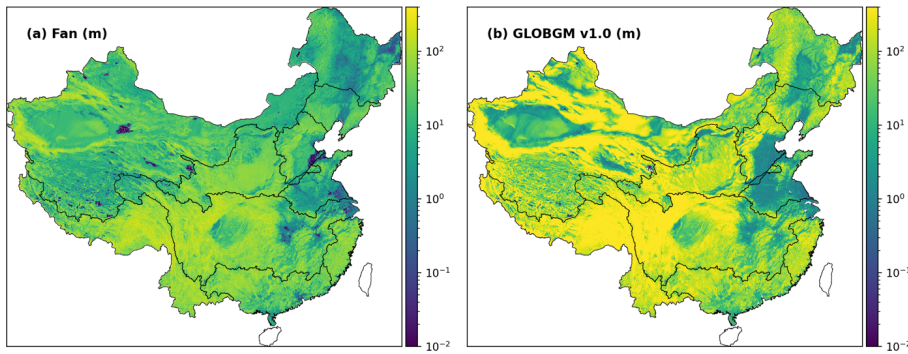
415
416   **Figure 6. Water table depths from two global models in CONCN 1.0 domain: (a) Fan's model**
417   **and (b) GLOBGM v1.0.**
418

419   We collected monthly observations of hydraulic head in 8563 wells in 2018. After removing

420   wells located out of the model domain, in confined aquifers, and on ParFlow river channels, 2436

421   wells remained for evaluation (Figure 7a). The annual means of WTD were calculated by

422   subtracting hydraulic heads from well elevations measured at the land surface. These wells are part

423   of the national groundwater monitoring network maintained by the Ministry of Land and

424   Resources. We collected the data by digitizing the China Geological Environmental Monitoring

425   Groundwater Level Yearbook of 2018 and then double-checked the data to avoid errors. The

426 yearbook, which started from 2005, has currently been updated to 2021. We fully understand that

427 one-year monthly observations cannot represent the long-term average state of water table. An

428 ongoing effort is being made to digitize all data in the yearbook and apply QA/QC (quality

429 assurance and quality control) on the digitized data, although it will take a few years to finish.

430   We compared WTDs simulated by the three models with observations (Figure 8). RSR values

431 show generally satisfied performances for all three models. CONCN 1.0 has RSR values that fall

432 between the two global models (0.88 compared to 0.80 and 1.41), with a bias towards shallow

433 water tables. The residuals of WTD for each model are shown in Figures 7b-d. Each subplot also

434 shows the decrease of groundwater storage based on GRACE data (Zhao et al., 2023), which is

435 classified into three levels: moderate, rapid, and dramatic. The decrease of groundwater storage is

436 mainly observed in Northern China, such as the Song-Liao Plains, the North China Plain, the Hetao

437 Plain, and the northern edge of Tarim Basin. Agriculture, with intensive groundwater pumping for

438 irrigation, is well-developed in these areas. While model simulations represent natural conditions

439 without groundwater pumping, simulated water tables might be expected to be shallower than

440 observed, i.e., negative WTD residuals, given anthropogenic impacts. However, the residuals from

441 the Fan et al. model show positive residuals in these areas (Figure 7c). Similarly, positive residuals

442 of GLOBGM v1.0 are found in Tibet and the Song-Liao Plains, where the decrease of groundwater

443 storage is likely significant. Given the uncertainty in groundwater pumping and the lack of

444 extraction data, it is challenging to represent these processes in large scale models. It is important

445 to note that Fan's model is an inverse model and the predecessor of GLOBGM v1.0 is a calibrated

446 model while the ParFlow CONCN 1.0 model is uncalibrated. Groundwater observations are sparse,

447 many uncertainties exist, particularly in the subsurface architecture, and extraction from wells is

448 unknown, creating a substantial modeling challenge. Calibration of large-scale groundwater

449 models to observations becomes particularly challenging given that both extraction and hydraulic

450 conductivity will lower water tables and can have an equal impact on RSR values.
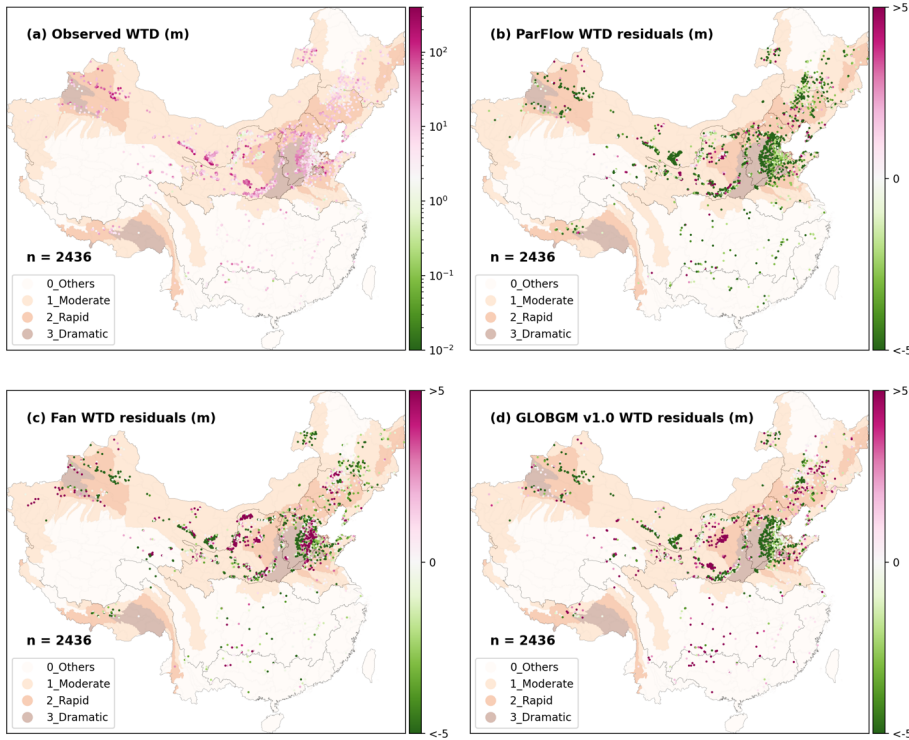
452
453 **Figure 7. Well locations (a) and residuals of water table depth for each model (b-d). Residuals**
454 **here refer to the differences between simulations and observations. The background shows**
455 **the average decrease of groundwater storage from 2003 to 2020 based on GRACE data (Zhao**
456 **et al., 2023). The decrease is classified into three levels: moderate, rapid, and dramatic.**
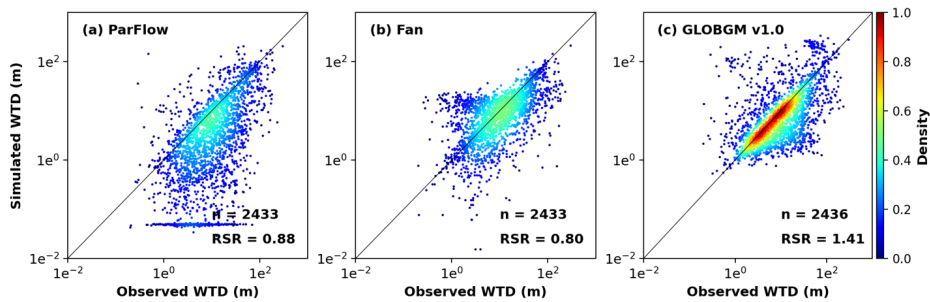
457
458 **Figure 8. Scatterplots of simulations vs. observations of water table depth. The simulations**
459 **are long-term average water table depths of 1981–2010 in current work, 2004–2014 in Fan's**
460 **model, and 1958–2015 in GLOBGM v1.0. The observations are the averages of 2018.**
461
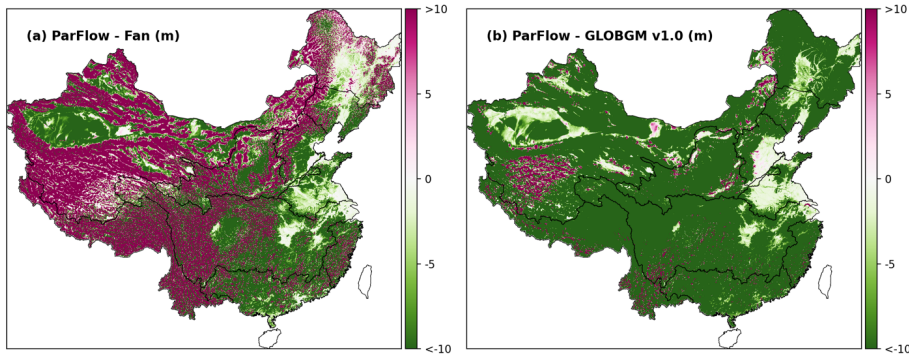
Figure 9. Differences of water table depth between CONCN 1.0 and two global models: (a) the difference between CONCN 1.0 and Fan's model and (b) the difference between CONCN 1.0 and GLOBGM v1.0.

5. Discussion

All three models show deep simulated water tables located just below the Szechwan Basin, at the boundaries of the Yangtze River and the Pearl River Basins (Figure 7). This finding may suggest a higher potential recharge in 2018 compared to the historic period (1981–2010), which was used to drive the model. Notably, these areas are part of the extensive Karst regions (Wang et al., 2019), where unique potential recharge and groundwater movement may occur along preferential flow pathways (e.g., fractures and conduits) (Hartmann et al., 2017). Given that ParFlow modeling has demonstrated acceptable performance in Karst regions in previous studies (Srivastava et al., 2014; Yang et al., 2023b), we did not apply specific adjustments to model inputs for these regions. However, we assigned higher hydraulic conductivities in Karst regions, assuming that Karst aquifers behave similarly to porous media at an approximate 1 km scale (i.e., the model resolution). This assumption may simplify the Karst geology and we acknowledge its limitations, as the simulated deep water-tables could also result from the underlying Karst geology. More specifically, wells are easily created in places lacking prominent Karst features, where local hydraulic conductivities are relatively lower. However, the higher effective hydraulic conductivity of a grid cell may generate deep water tables without representing such subgrid heterogeneities.

In southern China where it is wet, CONCN 1.0 shows shallow water tables, whereas Fan's model and GLOBGW v1.0 predict relatively deeper water tables (Figures 7b-d). These differences likely arise from the distinct model formulations. ParFlow integrates overland flow and

groundwater movement by simultaneously solving Richards' and shallow water equations via shared nodes in the top layer. As a result, WTDs in wells near rivers are likely underestimated, due to the widened rivers in the model, resulted from the model's resolution of approximately 1 km. WTDs in some wells located too close to rivers, e.g., tens or hundreds of meters which are smaller than the model resolution, cannot be captured at all, as the grid cell has been fully saturated. However, monitoring wells are typically located near rivers, which explains the shallow WTDs generated by CONCN 1.0 in southern China (Figure 7b). Fan's model and GLOBGW v1.0, which account for river-groundwater interactions, use the difference between groundwater head and river level (Fan et al., 2017; De Graaf et al., 2017). In these two models, rivers and the top subsurface layer are loosely coupled without shared pressure heads. In other words, rivers can flexibly carve the topography and groundwater with levels lower than the land surface can discharge to rivers. Additionally, WTDs, even in grid-cells with rivers, can be calibrated, which is not possible in ParFlow due to the integrated formulation. Though Fan's model and GLOBGW v1.0 use similar formulations for groundwater-river interactions, WTDs of Fan's model are shallower than those of GLOBGW v1.0 in southern China, which highlights other uncertainties of the two models (Reinecke et al., 2024).

To avoid the bias in evaluation caused by well locations as they are concentrated near rivers, we plotted the differences of WTDs between CONCN 1.0 and the two global models in Figures 9a-b. Results indicate that Fan's model generally produces shallower WTDs, whereas GLOBGW v1.0 simulates deeper WTDs, i.e., an intermediate performance of CONCN 1.0, which expands the understandings in riparian areas to the entire modeling domain. The significant discrepancies of WTDs across the three models highlight substantial uncertainties in WTDs simulated by current large-scale groundwater models, which cannot be fully revealed using the limited available observations. This underscores the need for further efforts in parameterizations and formulations of the models in this modeling community. Reinecke et al. (2024) found that WTDs generated by global models are strongly correlated with topography (i.e., slope) yet exhibit minimal climatic influences. In contrast, WTDs of Fan's model and observations show weaker correlations with topography and can be further differentiated in water-limited and energy-limited regions. We show generally similar results in Figure 10, where red and blue are used to differentiate the Spearman rank correlations and boxplots in wet and arid regions based on potential recharge in Figure 2f.
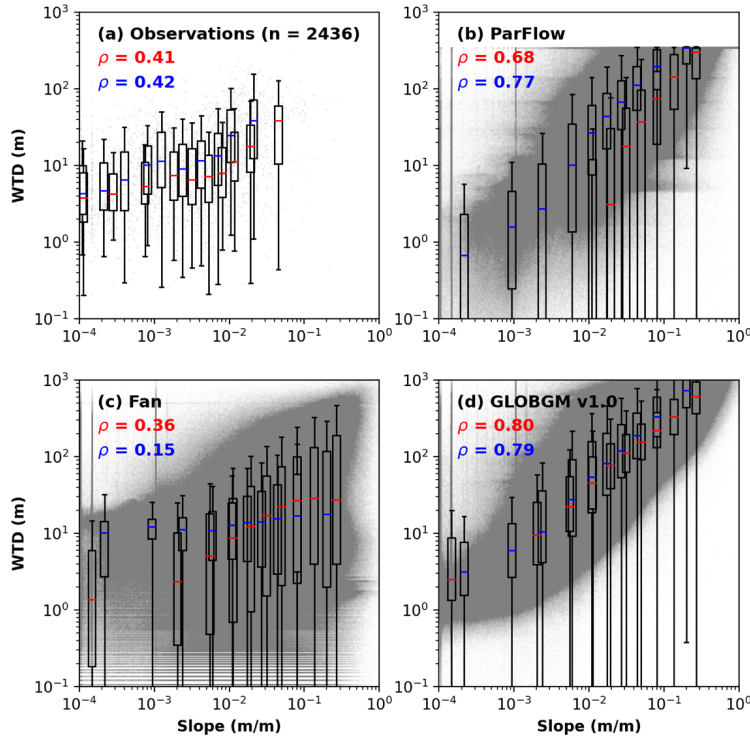
Figure 10. Variations of water table depth with topographic slope for observations (a) and simulations of three models (b-c). Spearman rank correlations shown in each subplot are based on the point cloud. Boxplots (without outliers) for better visualization of the point cloud are created by evenly separating slopes to ten bins. Boxplot and Spearman rank correlations in each subplot are distinguished by potential recharge. Red and blue are for points located in regions with and without long-term average potential recharge (i.e., P-ET>0 and P-ET=0).

In Figure 10, WTDs of CONCN 1.0 and GLOBGM v1.0 show strong correlations with topography, whereas observations and WTDs of Fan's model exhibit weaker correlations. The shallower WTDs simulated by ParFlow in wet regions, as discussed earlier, may decrease the correlation with topography, yet it is interesting to find that the terrain following grid of ParFlow results in slightly lower correlations than GLOBGM v1.0. Unlike the findings in Reinecke et al. (2024), correlations of observations with topography in different climate regions appear similar. This different finding could be attributed to the predominance of agricultural areas in the

observation dataset, where groundwater pumping likely exerts significant influence. The limited number of observations in this study is another potential limitation. In addition to the general explanation for the different correlations among models in Reinecke et al. (2024), the formulation of Fan's model may play an important role. By incorporating plant use of groundwater and dynamic root uptake depth in an inverse modeling based on inferred ET from remote sensing, Fan's model may introduce stronger regulations on water table via recharge, thereby diminishing the controls from (or the sensitivity to) topography. Additionally, Fan's model relies on remote sensing ET occurred under irrigation conditions, which includes the ET induced by irrigation. This additional ET is likely derived from groundwater, amplifying the effects of plant water use compared to natural conditions. This phenomenon may also explain the deeper water tables predicted by Fan's model in agricultural areas, as shown in Figure 7. These findings suggest that groundwater models should account for plant water use from deep soil or groundwater. Recharge estimated by hydrological or land-surface models with limited soil depths and/or without lateral groundwater convergence may be insufficient. Furthermore, uncertainties arising from human disturbances, such as groundwater pumping, should also be quantified.

6. Summary and forward outlook

In this study, we built the first surface water-groundwater integrated hydrologic modeling platform of the entire continental China with a high resolution using ParFlow. This CONCN 1.0 model was rigorously evaluated by both data products and observations, based on RSR values. Comparisons with observations show satisfied performances in streamflow and water table depth. Comparisons with global data products show comparable performance of streamflow to the global models and an intermediate performance of water table depth among global models. These results also demonstrate the transferability of the modeling workflow using ParFlow. However, we also recognize the challenges inherent in large scale hydrologic modeling. Data quality and/or availability (e.g., for direct use or quick access) presents a significant challenge during modeling. The vast arid and semi-arid regions of China further increase uncertainties in input data, such as potential recharge. As a result, lower simulated streamflow is observed in northwest China and in the Haihe and Liao River Basins. Significant uncertainties in simulated water table depth are identified in current large-scale groundwater models, which might be attributed to the different parameterizations and formulations of the models, necessitating continuous efforts from the community.

566   We hope that our work can catalyze conversations and collaborations between various
567 communities involved in hydrologic modeling, geological surveys, model development, data
568 products, and data monitoring/sharing. Clearly, all efforts are aimed at improving the efficiencies
569 and capabilities of large-scale hydrologic modeling, which is powerful to address diverse
570 ecohydrologic issues and accelerate scientific discoveries across multiple disciplines. Below, we
571 summarize both the challenges and opportunities that require the attention and collaborative efforts
572 of the hydrology community and beyond.

573   (1) Human activities related to water resources are intensive in China, such as the long-term
574   groundwater pumping in Huang-Huai-Hai plains, the South-North water transfer projects,
575   the operation of the Three Gorges Dam, and the revegetation in the Loess Plateau. Flash
576   extremes are also becoming more frequent, such as the Yangtze drought (August 2022) and
577   the storms in Zhengzhou (July 2022) and Beijing (July 2023). These factors make China
578   one of the world's most significant ecohydrologic hotspots. Integrated hydrologic
579   modeling systems are essential to address these issues. While local and regional models
580   have been developed in recent years, modeling platforms with high resolution at larger or
581   national scales are still lacking, hindering efficient water resources management and timely
582   decision-making across multiple scales.

583   (2) Hydrologic processes, especially groundwater at the hillslope or catchment scales, play
584   important roles in terrestrial water and energy cycles, yet they are often oversimplified or
585   poorly represented in Earth system models. Many studies conducted in China on critical
586   hydrologic questions have focused on limited components of the hydrologic cycle.
587   Therefore, it is urgent to build large-scale hydrologic models and couple them with regional
588   weather or climatic models to better understand the terrestrial hydrologic cycle in China.
589   More importantly, the modeling should go beyond water balance to include flow paths or
590   water quality to gain a deeper understanding of the food-energy-water nexus and to conduct
591   risk assessment in the changing world.

592   (3) Large-scale hydrologic modeling relies on massive amounts of data for various input
593   variables. Discrete observations are often not user-friendly for direct use by modelers. Data
594   products help fill spatial and temporal gaps and are necessary for effective modeling. Many
595   of the products currently used only emerged in recent years, making large-scale hydrologic
596   modeling inefficient in China and other parts of the world in earlier times. The rapid

597   development of global data products suggests that now it is the ideal time to build large-
598   scale, consistent hydrologic modeling platforms. However, high-quality data products
599   within a consistent framework are still lacking and inter-evaluations between different
600   products could help constrain uncertainties from various sources (see section 2.3).

601   (4) We also need to leverage the strengths of local documents in China. The hydrolithologies
602   of GLHYMPS 1.0 were built using the global lithology map GLiM, which relies on the
603   geological map with a scale of 1:2.5 million published by China Geological Survey in 2001.
604   Currently, national geological maps with a scale of 1:500,000 are available, while some
605   local maps have the scale to 1:50,000. We need to fully consider such resources to improve
606   the permeability/hydrolithology products in China in terms of both horizontal resolution
607   and available depth. This is critical for building a more reliable hydrostratigraphy, which
608   could substantially improve model performance. In addition, much useful information is
609   probably hidden in system conceptualizations done for previous modelling studies. We
610   should consciously investigate, accumulate, and utilize this information. Particularly in the
611   context of groundwater system, hydrogeologists may have interpreted available data in
612   many places before, which holds valuable information due to the regional combination of
613   expertise and data.

614   (5) Building large-scale hydrologic models using different formulations is encouraged. Model
615   comparisons are necessary to identify the strengths and limitations of different modeling
616   systems on focus issues (Bailey et al., 2016; Zafarmomen et al., 2024; Kim et al., 2008).
617   Such community activities are also helpful in reaching consensus on critical questions,
618   such as conceptual models or model parameterizations, calibrations, evaluations, and
619   opportunities incorporating new techniques and concepts. All of these factors are essential
620   for improving the performance of next-generation models in China and can provide
621   valuable insights for modeling efforts in other parts of the world.

622

Data and code availability

624   Datasets we used are all from public sources and have been cited in the main text. The ParFlow
625   Version 3.12–3.13 we used can be found here: https://doi.org/10.5281/zenodo.4816884

Author contributions

633 Conceptualization: CY and RM. Methodology: CY, LC, and RM. Investigation: CY, ZJ, WX,
634 and RM. Resources: ZW, XZ, YZ, YD, and RM. Writing – original draft: CY. Writing – review
635 and editing: CY, JM, and RM.

Competing interests

637 The authors have declared that there are no competing interests.

Acknowledgements

639 We are pleased to acknowledge that the work reported in this paper was substantially
640 performed using the Princeton Research Computing resources at Princeton University which is a
641 consortium of groups led by the Princeton Institute for Computational Science and Engineering
642 (PICSciE) and the Office of Information Technology's Research Computing. We would like to
643 acknowledge the high-performance computing support from Derecho provided by NCAR's
644 Computational and Information Systems Laboratory.

References

646 Bailey, R. T., Wible, T. C., Arabi, M., Records, R. M., and Ditty, J.: Assessing regional-scale spatio-
647   temporal patterns of groundwater–surface water interactions using a coupled SWAT-
648   MODFLOW model, Hydrol Process, 30, 4420-4433, https://doi.org/10.1002/hyp.10933, 2016.
649 Belleflamme, A., Goergen, K., Wagner, N., Kollet, S., Bathiany, S., El Zohbi, J., Rechid, D.,
650   Vanderborght, J., and Vereecken, H.: Hydrological forecasting at impact scale: the integrated
651   ParFlow hydrological model at 0.6 km for climate resilient water resource management over
652   Germany, Frontiers in Water, 5, 10.3389/frwa.2023.1183642, 2023.
653 Bianchi, M., Scheidegger, J., Hughes, A., Jackson, C., Lee, J., Lewis, M., Mansour, M., Newell,
654   A., O'Dochartaigh, B., Patton, A., and Dadson, S.: Simulation of national-scale groundwater
655   dynamics in geologically complex aquifer systems: an example from Great Britain,
656   Hydrological Sciences Journal, 69, 572-591, 10.1080/02626667.2024.2320847, 2024.
657 Cao, G. L., Zheng, C. M., Scanlon, B. R., Liu, J., and Li, W. P.: Use of flow modeling to assess
658   sustainability of groundwater resources in the North China Plain, Water Resour Res, 49, 159-
659   175, 10.1029/2012wr011899, 2013.
660 Chen, J., Sudicky, E. A., Davison, J. H., Frey, S. K., Park, Y. J., Hwang, H. T., Erler, A. R., Berg,
661   S. J., Callaghan, M. V., Miller, K., Ross, M., and Peltier, W. R.: Towards a climate-driven
662   simulation of coupled surface-subsurface hydrology at the continental scale: a Canadian
663   example, Canadian Water Resources Journal / Revue canadienne des ressources hydriques, 45,
664   11-27, 10.1080/07011784.2019.1671235, 2020.
665 Collins, G. and Reddy, G.: China's Growing Water Crisis, Foreign Affairs, 2022.
666 Condon, L. E. and Maxwell, R. M.: Modified priority flood and global slope enforcement
667   algorithm for topographic processing in physically based hydrologic modeling applications,
668   Comput Geosci-Uk, 126, 73-83, 10.1016/j.cageo.2019.01.020, 2019.
669 Condon, L. E., Kollet, S., Bierkens, M. F. P., Fogg, G. E., Maxwell, R. M., Hill, M. C., Fransen,
670   H.-J. H., Verhoef, A., Van Loon, A. F., Sulis, M., and Abesser, C.: Global Groundwater

Modeling and Monitoring: Opportunities and Challenges, Water Resour Res, 57, e2020WR029500, https://doi.org/10.1029/2020WR029500, 2021.

Cosgrove, B., Gochis, D., Flowers, T., Dugger, A., Ogden, F., Graziano, T., Clark, E., Cabell, R., Casiday, N., Cui, Z., Eicher, K., Fall, G., Feng, X., Fitzgerald, K., Frazier, N., George, C., Gibbs, R., Hernandez, L., Johnson, D., Jones, R., Karsten, L., Kefelegn, H., Kitzmiller, D., Lee, H., Liu, Y., Mashriqui, H., Mattern, D., McCluskey, A., McCreight, J. L., McDaniel, R., Midekisa, A., Newman, A., Pan, L., Pham, C., RafieeiNasab, A., Rasmussen, R., Read, L., Rezaeianzadeh, M., Salas, F., Sang, D., Sampson, K., Schneider, T., Shi, Q., Sood, G., Wood, A., Wu, W., Yates, D., Yu, W., and Zhang, Y.: NOAA's National Water Model: Advancing operational hydrology through continental-scale modeling, JAWRA Journal of the American Water Resources Association, 60, 247-272, https://doi.org/10.1111/1752-1688.13184, 2024.

Dai, Y., Xin, Q., Wei, N., Zhang, Y., Shangguan, W., Yuan, H., Zhang, S., Liu, S., and Lu, X.: A Global High-Resolution Data Set of Soil Hydraulic and Thermal Properties for Land Surface Modeling, J Adv Model Earth Sy, 11, 2996-3023, 10.1029/2019ms001784, 2019.

Dai, Y. J., Zeng, X. B., Dickinson, R. E., Baker, I., Bonan, G. B., Bosilovich, M. G., Denning, A. S., Dirmeyer, P. A., Houser, P. R., Niu, G. Y., Oleson, K. W., Schlosser, C. A., and Yang, Z. L.: The Common Land Model, B Am Meteorol Soc, 84, 1013-1023, 10.1175/Bams-84-8-1013, 2003.

David, C. H., Maidment, D. R., Niu, G.-Y., Yang, Z.-L., Habets, F., and Eijkhout, V.: River Network Routing on the NHDPlus Dataset, J Hydrometeorol, 12, 913-934, https://doi.org/10.1175/2011JHM1345.1, 2011.

de Graaf, I., Condon, L., and Maxwell, R.: Hyper-Resolution Continental-Scale 3-D Aquifer Parameterization for Groundwater Modeling, Water Resour Res, 56, e2019WR026004, https://doi.org/10.1029/2019WR026004, 2020.

de Graaf, I. E. M., Sutanudjaja, E. H., van Beek, L. P. H., and Bierkens, M. F. P.: A high-resolution global-scale groundwater model, Hydrol Earth Syst Sc, 19, 823-837, 10.5194/hess-19-823-2015, 2015.

de Graaf, I. E. M., van Beek, R. L. P. H., Gleeson, T., Moosdorf, N., Schmitz, O., Sutanudjaja, E. H., and Bierkens, M. F. P.: A global-scale two-layer transient groundwater model: Development and application to groundwater depletion, Adv Water Resour, 102, 53-67, https://doi.org/10.1016/j.advwatres.2017.01.011, 2017.

Delsman, J. R., Mulder, T., Romero Verastegui, B., Bootsma, H., Zitman, P., Huizer, S., and Oude Essink, G. H. P.: Reproducible construction of a high-resolution national variable-density groundwater salinity model for the Netherlands, Environ Modell Softw, 164, 105683, https://doi.org/10.1016/j.envsoft.2023.105683, 2023.

Devitt, L., Neal, J., Wagener, T., and Coxon, G.: Uncertainty in the extreme flood magnitude estimates of large-scale flood hazard models, Environ Res Lett, 16, 064013, 10.1088/1748-9326/abfac4, 2021.

Eilander, D., van Verseveld, W., Yamazaki, D., Weerts, A., Winsemius, H. C., and Ward, P. J.: A hydrography upscaling method for scale-invariant parametrization of distributed hydrological models, Hydrol. Earth Syst. Sci., 25, 5287-5313, 10.5194/hess-25-5287-2021, 2021.

Fan, Y., Li, H., and Miguez-Macho, G.: Global Patterns of Groundwater Table Depth, Science, 339, 940-943, 10.1126/science.1229881, 2013.

Fan, Y., Miguez-Macho, G., Jobbágy, E. G., Jackson, R. B., and Otero-Casal, C.: Hydrologic regulation of plant rooting depth, Proceedings of the National Academy of Sciences, 114, 10572-10577, 10.1073/pnas.1712381114, 2017.

Fan, Y., Miguez-Macho, G., Weaver, C. P., Walko, R., and Robock, A.: Incorporating water table dynamics in climate modeling: 1. Water table observations and equilibrium water table simulations, Journal of Geophysical Research: Atmospheres, 112, https://doi.org/10.1029/2006JD008111, 2007.

Feng, D., Fang, K., and Shen, C.: Enhancing Streamflow Forecast and Extracting Insights Using Long-Short Term Memory Networks With Data Integration at Continental Scales, Water Resour Res, 56, e2019WR026793, https://doi.org/10.1029/2019WR026793, 2020.

Ferguson, G., McIntosh, J. C., Jasechko, S., Kim, J.-H., Famiglietti, J. S., and McDonnell, J. J.: Groundwater deeper than 500 m contributes less than 0.1% of global river discharge, Commun Earth Environ, 4, 48, 10.1038/s43247-023-00697-6, 2023.

Foster, L. M., Williams, K. H., and Maxwell, R. M.: Resolution matters when modeling climate change in headwaters of the Colorado River, Environ Res Lett, 15, 104031, 10.1088/1748-9326/aba77f, 2020.

Friedl, M. and Sulla-Menashe, D.: MODIS/Terra+Aqua Land Cover Type Yearly L3 Global 500m SIN Grid V061, NASA EOSDIS Land Processes Distributed Active Archive Center [dataset], https://doi.org/10.5067/MODIS/MCD12Q1.061, 2022.

Gleeson, T., Moosdorf, N., Hartmann, J., and van Beek, L. P. H.: A glimpse beneath earth's surface: GLobal HYdrogeology MaPS (GLHYMPS) of permeability and porosity, Geophys Res Lett, 41, 3891-3898, 10.1002/2014gl059856, 2014.

Gleeson, T., Wagener, T., Döll, P., Zipper, S. C., West, C., Wada, Y., Taylor, R., Scanlon, B., Rosolem, R., Rahman, S., Oshinlaja, N., Maxwell, R., Lo, M. H., Kim, H., Hill, M., Hartmann, A., Fogg, G., Famiglietti, J. S., Ducharne, A., de Graaf, I., Cuthbert, M., Condon, L., Bresciani, E., and Bierkens, M. F. P.: GMD perspective: The quest to improve the evaluation of groundwater representation in continental- to global-scale models, Geosci. Model Dev., 14, 7545-7571, 10.5194/gmd-14-7545-2021, 2021.

Gochis, D. J., Yu, W., and Yates, D. N.: The WRF-Hydro model technical description and user's guide, version 3.0, NCAR Technical Document, 120 pages, 2015.

Han, J., Miao, C., Gou, J., Zheng, H., Zhang, Q., and Guo, X.: A new daily gridded precipitation dataset for the Chinese mainland based on gauge observations, Earth Syst. Sci. Data, 15, 3147-3161, 10.5194/essd-15-3147-2023, 2023.

Hartmann, A., Gleeson, T., Wada, Y., and Wagener, T.: Enhanced groundwater recharge rates and altered recharge sensitivity to climate variability through subsurface heterogeneity, Proceedings of the National Academy of Sciences, 114, 2842-2847, doi:10.1073/pnas.1614941114, 2017.

Hartmann, J. and Moosdorf, N.: The new global lithological map database GLiM: A representation of rock properties at the Earth surface, Geochemistry, Geophysics, Geosystems, 13, https://doi.org/10.1029/2012GC004370, 2012.

Hellwig, J., de Graaf, I. E. M., Weiler, M., and Stahl, K.: Large-Scale Assessment of Delayed Groundwater Responses to Drought, Water Resour Res, 56, e2019WR025441, https://doi.org/10.1029/2019WR025441, 2020.

Henriksen, H. J., Troldborg, L., Nyegaard, P., Sonnenborg, T. O., Refsgaard, J. C., and Madsen, B.: Methodology for construction, calibration and validation of a national hydrological model for Denmark, J Hydrol, 280, 52-71, https://doi.org/10.1016/S0022-1694(03)00186-0, 2003.

Hoch, J. M., Sutanudjaja, E. H., Wanders, N., van Beek, R. L. P. H., and Bierkens, M. F. P.: Hyper-resolution PCR-GLOBWB: opportunities and challenges from refining model spatial

resolution to 1 km over the European continent, Hydrol. Earth Syst. Sci., 27, 1383-1401, 10.5194/hess-27-1383-2023, 2023.

Hu, L., Xu, Z., and Huang, W.: Development of a river-groundwater interaction model and its application to a catchment in Northwestern China, J Hydrol, 543, 483-500, https://doi.org/10.1016/j.jhydrol.2016.10.028, 2016.

Huang, C., Zheng, X., Tait, A., Dai, Y., Yang, C., Chen, Z., Li, T., and Wang, Z.: On using smoothing spline and residual correction to fuse rain gauge observations and remote sensing data, J Hydrol, 508, 410-417, https://doi.org/10.1016/j.jhydrol.2013.11.022, 2014.

Huscroft, J., Gleeson, T., Hartmann, J., and Börker, J.: Compiling and Mapping Global Permeability of the Unconsolidated and Consolidated Earth: GLobal HYdrogeology MaPS 2.0 (GLHYMPS 2.0), Geophys Res Lett, 45, 1897-1904, https://doi.org/10.1002/2017GL075860, 2018.

Jiang, X., Ma, R., Ma, T., and Sun, Z.: Modeling the effects of water diversion projects on surface water and groundwater interactions in the central Yangtze River basin, Sci Total Environ, 830, 154606, https://doi.org/10.1016/j.scitotenv.2022.154606, 2022.

Jiang, Y.: China's water scarcity, Journal of Environmental Management, 90, 3185-3196, https://doi.org/10.1016/j.jenvman.2009.04.016, 2009.

Jiménez, C., Prigent, C., Mueller, B., Seneviratne, S. I., McCabe, M. F., Wood, E. F., Rossow, W. B., Balsamo, G., Betts, A. K., Dirmeyer, P. A., Fisher, J. B., Jung, M., Kanamitsu, M., Reichle, R. H., Reichstein, M., Rodell, M., Sheffield, J., Tu, K., and Wang, K.: Global intercomparison of 12 land surface heat flux estimates, Journal of Geophysical Research: Atmospheres, 116, https://doi.org/10.1029/2010JD014545, 2011.

Kim, N. W., Chung, I. M., Won, Y. S., and Arnold, J. G.: Development and application of the integrated SWAT–MODFLOW model, J Hydrol, 356, 1-16, https://doi.org/10.1016/j.jhydrol.2008.02.024, 2008.

Knoben, W. J. M., Freer, J. E., and Woods, R. A.: Technical note: Inherent benchmark or not? Comparing Nash–Sutcliffe and Kling–Gupta efficiency scores, Hydrol. Earth Syst. Sci., 23, 4323-4331, 10.5194/hess-23-4323-2019, 2019.

Kollet, S. J. and Maxwell, R. M.: Integrated surface-groundwater flow modeling: A free-surface overland flow boundary condition in a parallel groundwater flow model, Adv Water Resour, 29, 945-958, 2006.

Kollet, S. J. and Maxwell, R. M.: Capturing the influence of groundwater dynamics on land surface processes using an integrated, distributed watershed model, Water Resour Res, 44, Artn W0240210.1029/2007wr006004, 2008.

Lancia, M., Yao, Y., Andrews, C. B., Wang, X., Kuang, X., Ni, J., Gorelick, S. M., Scanlon, B. R., Wang, Y., and Zheng, C.: The China groundwater crisis: A mechanistic analysis with implications for global sustainability, Sustainable Horizons, 4, 100042, https://doi.org/10.1016/j.horiz.2022.100042, 2022.

Li, Z., Chen, Y., Yang, J., and Wang, Y.: Potential evapotranspiration and its attribution over the past 50 years in the arid region of Northwest China, Hydrol Process, 28, 1025-1031, https://doi.org/10.1002/hyp.9643, 2014.

Lin, P., Pan, M., Beck, H. E., Yang, Y., Yamazaki, D., Frasson, R., David, C. H., Durand, M., Pavelsky, T. M., Allen, G. H., Gleason, C. J., and Wood, E. F.: Global Reconstruction of Naturalized River Flows at 2.94 Million Reaches, Water Resour Res, 55, 6499-6516, 10.1029/2019wr025287, 2019.

807 Livneh, B., Bohn, T. J., Pierce, D. W., Munoz-Arriola, F., Nijssen, B., Vose, R., Cayan, D. R., and
808   Brekke, L.: A spatially comprehensive, hydrometeorological data set for Mexico, the U.S., and
809   Southern Canada 1950–2013, Sci Data, 2, 150042, 10.1038/sdata.2015.42, 2015.
810 Ma, N., Szilagyi, J., Zhang, Y., and Liu, W.: Complementary-Relationship-Based Modeling of
811   Terrestrial Evapotranspiration Across China During 1982–2012: Validations and
812   Spatiotemporal Analyses, Journal of Geophysical Research: Atmospheres, 124, 4326-4351,
813   https://doi.org/10.1029/2018JD029850, 2019.
814 Maxwell, R. M.: A terrain-following grid transform and preconditioner for parallel, large-scale,
815   integrated hydrologic modeling, Adv Water Resour, 53, 109-117,
816   https://doi.org/10.1016/j.advwatres.2012.10.001, 2013.
817 Maxwell, R. M., Condon, L. E., and Kollet, S. J.: A high-resolution simulation of groundwater and
818   surface water over most of the continental US with the integrated hydrologic model ParFlow
819   v3, Geosci Model Dev, 8, 923-937, 10.5194/gmd-8-923-2015, 2015.
820 Miao, C., Gou, J., Fu, B., Tang, Q., Duan, Q., Chen, Z., Lei, H., Chen, J., Guo, J., Borthwick, A.
821   G. L., Ding, W., Duan, X., Li, Y., Kong, D., Guo, X., and Wu, J.: High-quality reconstruction
822   of China's natural streamflow, Science Bulletin, 67, 547-556,
823   https://doi.org/10.1016/j.scib.2021.09.022, 2022.
824 Müller Schmied, H., Cáceres, D., Eisner, S., Flörke, M., Herbert, C., Niemann, C., Peiris, T. A.,
825   Popat, E., Portmann, F. T., Reinecke, R., Schumacher, M., Shadkam, S., Telteu, C. E.,
826   Trautmann, T., and Döll, P.: The global water resources and use model WaterGAP v2.2d: model
827   description and evaluation, Geosci. Model Dev., 14, 1037-1079, 10.5194/gmd-14-1037-2021,
828   2021.
829 Muñoz-Sabater, J., Dutra, E., Agustí-Panareda, A., Albergel, C., Arduini, G., Balsamo, G.,
830   Boussetta, S., Choulga, M., Harrigan, S., Hersbach, H., Martens, B., Miralles, D. G., Piles, M.,
831   Rodríguez-Fernández, N. J., Zsoter, E., Buontempo, C., and Thépaut, J. N.: ERA5-Land: a
832   state-of-the-art global reanalysis dataset for land applications, Earth Syst. Sci. Data, 13, 4349-
833   4383, 10.5194/essd-13-4349-2021, 2021.
834 N. Moriasi, D., G. Arnold, J., W. Van Liew, M., L. Bingner, R., D. Harmel, R., and L. Veith, T.:
835   Model Evaluation Guidelines for Systematic Quantification of Accuracy in Watershed
836   Simulations, Transactions of the ASABE, 50, 885-900, https://doi.org/10.13031/2013.23153,
837   2007.
838 Niu, Z., He, H., Zhu, G., Ren, X., Zhang, L., and Zhang, K.: A spatial-temporal continuous dataset
839   of the transpiration to evapotranspiration ratio in China from 1981–2015, Sci Data, 7, 369,
840   10.1038/s41597-020-00693-x, 2020.
841 O'Neill, M. M. F., Tijerina, D. T., Condon, L. E., and Maxwell, R. M.: Assessment of the ParFlow–
842   CLM CONUS 1.0 integrated hydrologic model: evaluation of hyper-resolution water balance
843   components across the contiguous United States, Geosci. Model Dev., 14, 7223-7254,
844   10.5194/gmd-14-7223-2021, 2021.
845 Peng, S.: 1-km monthly precipitation dataset for China (1901-2022), National Tibetan Plateau Data
846   Center [dataset], 10.5281/zenodo.3185722, 2020.
847 Pietz, D. A.: China's Water Challenges: National and Global Implications, Education About ASIA,
848   22, 8-14, 2017.
849 Regan, R. S., Juracek, K. E., Hay, L. E., Markstrom, S. L., Viger, R. J., Driscoll, J. M., LaFontaine,
850   J. H., and Norton, P. A.: The U. S. Geological Survey National Hydrologic Model infrastructure:
851   Rationale, description, and application of a watershed-scale model for the conterminous United

852 States, Environ Modell Softw, 111, 192-203, https://doi.org/10.1016/j.envsoft.2018.09.023,
853 2019.
854 Reinecke, R., Foglia, L., Mehl, S., Trautmann, T., Cáceres, D., and Döll, P.: Challenges in
855 developing a global gradient-based groundwater model (G3M v1.0) for the integration into a
856 global hydrological model, Geosci. Model Dev., 12, 2401-2418, 10.5194/gmd-12-2401-2019,
857 2019.
858 Reinecke, R., Wachholz, A., Mehl, S., Foglia, L., Niemann, C., and Döll, P.: Importance of Spatial
859 Resolution in Global Groundwater Modeling, Groundwater, 58, 363-376,
860 https://doi.org/10.1111/gwat.12996, 2020.
861 Reinecke, R., Gnann, S., Stein, L., Bierkens, M., de Graaf, I., Gleeson, T., Essink, G. O.,
862 Sutanudjaja, E. H., Ruz Vargas, C., Verkaik, J., and Wagener, T.: Uncertainty in model
863 estimates of global groundwater depth, Environ Res Lett, 19, 114066, 10.1088/1748-
864 9326/ad8587, 2024.
865 Running, S., Mu, Q., Zhao, M., and Moreno, A.: MODIS/Terra Net Evapotranspiration Gap-Filled
866 Yearly L4 Global 500m SIN Grid V061, NASA EOSDIS Land Processes Distributed Active
867 Archive Center [dataset], https://doi.org/10.5067/MODIS/MOD16A3GF.061, 2021.
868 Schaap, M. G. and Leij, F. J.: Database-related accuracy and uncertainty of pedotransfer functions,
869 Soil science, v. 163, pp. 765-779-1998 v.1163 no.1910, 10.1097/00010694-199810000-00001,
870 1998.
871 Schaefli, B. and Gupta, H. V.: Do Nash values have value?, Hydrol Process, 21, 2075-2080,
872 https://doi.org/10.1002/hyp.6825, 2007.
873 Shangguan, W., Hengl, T., de Jesus, J. M., Yuan, H., and Dai, Y. J.: Mapping the global depth to
874 bedrock for land surface modeling, J Adv Model Earth Sy, 9, 65-88, 2017.
875 Srivastava, V., Graham, W., Muñoz-Carpena, R., and Maxwell, R. M.: Insights on geologic and
876 vegetative controls over hydrologic behavior of a large complex basin – Global Sensitivity
877 Analysis of an integrated parallel hydrologic model, J Hydrol, 519, 2238-2257,
878 https://doi.org/10.1016/j.jhydrol.2014.10.020, 2014.
879 Strahler, A. N.: Quantitative analysis of watershed geomorphology, Eos, Transactions American
880 Geophysical Union, 38, 913-920, https://doi.org/10.1029/TR038i006p00913, 1957.
881 Sutanudjaja, E. H., van Beek, R., Wanders, N., Wada, Y., Bosmans, J. H. C., Drost, N., van der Ent,
882 R. J., de Graaf, I. E. M., Hoch, J. M., de Jong, K., Karssenberg, D., López López, P.,
883 Peßenteiner, S., Schmitz, O., Straatsma, M. W., Vannametee, E., Wisser, D., and Bierkens, M.
884 F. P.: PCR-GLOBWB 2: a 5 arcmin global hydrological and water resources model,
885 Geosci. Model Dev., 11, 2429-2453, 10.5194/gmd-11-2429-2018, 2018.
886 Swilley, J. S., Tijerina-Kreuzer, D., Tran, H. V., Zhang, J., Yang, C., Condon, L. E., and Maxwell,
887 R. M.: Continental Scale Hydrostratigraphy: Comparing Geologically Informed Data Products
888 to Analytical Solutions, Groundwater, n/a, https://doi.org/10.1111/gwat.13354, 2023.
889 Tian, Y., Zheng, Y., Zheng, C., Xiao, H., Fan, W., Zou, S., Wu, B., Yao, Y., Zhang, A., and Liu, J.:
890 Exploring scale-dependent ecohydrological responses in a large endorheic river basin through
891 integrated surface water-groundwater modeling, Water Resour Res, 51, 4065-4085,
892 https://doi.org/10.1002/2015WR016881, 2015.
893 Tijerina, D., Condon, L., FitzGerald, K., Dugger, A., O'Neill, M. M., Sampson, K., Gochis, D.,
894 and Maxwell, R.: Continental Hydrologic Intercomparison Project, Phase 1: A Large-Scale
895 Hydrologic Model Comparison Over the Continental United States, Water Resour Res, 57,
896 e2020WR028931, https://doi.org/10.1029/2020WR028931, 2021.

Tijerina-Kreuzer, D., Swilley, J. S., Tran, H. V., Zhang, J., West, B., Yang, C., Condon, L. E., and Maxwell, R. M.: Continental scale hydrostratigraphy: basin-scale testing of alternative data-driven approaches, Groundwater, n/a, https://doi.org/10.1111/gwat.13357, 2023.

Vergnes, J.-P., Caballero, Y., and Lanini, S.: Assessing climate change impact on French groundwater resources using a spatially distributed hydrogeological model, Hydrological Sciences Journal, 68, 209-227, 10.1080/02626667.2022.2150553, 2023.

Verkaik, J., Sutanudjaja, E. H., Oude Essink, G. H. P., Lin, H. X., and Bierkens, M. F. P.: GLOBGM v1.0: a parallel implementation of a 30 arcsec PCR-GLOBWB-MODFLOW global-scale groundwater model, Geosci. Model Dev., 17, 275-300, 10.5194/gmd-17-275-2024, 2024.

Wang, K., Zhang, C., Chen, H., Yue, Y., Zhang, W., Zhang, M., Qi, X., and Fu, Z.: Karst landscapes of China: patterns, ecosystem processes and services, Landscape Ecology, 34, 2743-2763, 10.1007/s10980-019-00912-w, 2019.

Wang, X., Tian, Y., Yu, J., Lancia, M., Chen, J., Xiao, K., Zheng, Y., Andrews, C. B., and Zheng, C.: Complex Effects of Tides on Coastal Groundwater Revealed by High-Resolution Integrated Flow Modeling, Water Resour Res, 59, e2022WR033942, https://doi.org/10.1029/2022WR033942, 2023.

Westerhoff, R., White, P., and Miguez-Macho, G.: Application of an improved global-scale groundwater model for water table estimation across New Zealand, Hydrol. Earth Syst. Sci., 22, 6449-6472, 10.5194/hess-22-6449-2018, 2018.

Yamazaki, D., Ikeshima, D., Sosa, J., Bates, P. D., Allen, G. H., and Pavelsky, T. M.: MERIT Hydro: A High-Resolution Global Hydrography Map Based on Latest Topography Dataset, Water Resour Res, 55, 5053-5073, 10.1029/2019wr024873, 2019.

Yan, F., Shangguan, W., Zhang, J., and Hu, B.: Depth-to-bedrock map of China at a spatial resolution of 100 meters, Sci Data, 7, 2, 10.1038/s41597-019-0345-6, 2020.

Yang, C., Maxwell, R., McDonnell, J., Yang, X., and Tijerina-Kreuzer, D.: The Role of Topography in Controlling Evapotranspiration Age, Journal of Geophysical Research: Atmospheres, 128, e2023JD039228, https://doi.org/10.1029/2023JD039228, 2023a.

Yang, C., Tijerina-Kreuzer, D. T., Tran, H. V., Condon, L. E., and Maxwell, R. M.: A high-resolution, 3D groundwater-surface water simulation of the contiguous US: Advances in the integrated ParFlow CONUS 2.0 modeling platform, J Hydrol, 130294, https://doi.org/10.1016/j.jhydrol.2023.130294, 2023b.

Yang, C., Li, H.-Y., Fang, Y., Cui, C., Wang, T., Zheng, C., Leung, L. R., Maxwell, R. M., Zhang, Y.-K., and Yang, X.: Effects of Groundwater Pumping on Ground Surface Temperature: A Regional Modeling Study in the North China Plain, Journal of Geophysical Research: Atmospheres, 125, e2019JD031764, 10.1029/2019jd031764, 2020.

Yang, J. and Huang, X.: The 30 m annual land cover dataset and its dynamics in China from 1990 to 2019, Earth Syst. Sci. Data, 13, 3907-3925, 10.5194/essd-13-3907-2021, 2021.

Yang, Y., Feng, D., Beck, H. E., Hu, W., Sengupta, A., Monache, L. D., Hartman, R., Lin, P., Shen, C., and Pan, M.: Global Daily Discharge Estimation Based on Grid-Scale Long Short-Term Memory (LSTM) Model and River Routing, ESS Open Archive, DOI: 10.22541/essoar.169724927.73813721/v1, 2023c.

Yin, Z., Lin, P., Riggs, R., Allen, G. H., Lei, X., Zheng, Z., and Cai, S.: A synthesis of Global Streamflow Characteristics, Hydrometeorology, and Catchment Attributes (GSHA) for large sample river-centric studies, Earth Syst. Sci. Data, 16, 1559-1587, 10.5194/essd-16-1559-2024, 2024.

Yu, X., Luo, L., Hu, P., Tu, X., Chen, X., and Wei, J.: Impacts of sea-level rise on groundwater inundation and river floods under changing climate, J Hydrol, 614, 128554, https://doi.org/10.1016/j.jhydrol.2022.128554, 2022.

Zafarmomen, N., Alizadeh, H., Bayat, M., Ehtiat, M., and Moradkhani, H.: Assimilation of Sentinel-Based Leaf Area Index for Modeling Surface-Ground Water Interactions in Irrigation Districts, Water Resour Res, 60, e2023WR036080, https://doi.org/10.1029/2023WR036080, 2024.

Zhang, J., Condon, L. E., Tran, H., and Maxwell, R. M.: A national topographic dataset for hydrological modeling over the contiguous United States, Earth Syst. Sci. Data, 13, 3263-3279, 10.5194/essd-13-3263-2021, 2021.

Zhang, Y., Kong, D., Gan, R., Chiew, F. H. S., McVicar, T. R., Zhang, Q., and Yang, Y.: Coupled estimation of 500 m and 8-day resolution global evapotranspiration and gross primary production in 2002–2017, Remote Sens Environ, 222, 165-182, https://doi.org/10.1016/j.rse.2018.12.031, 2019.

Zhao, K., Fang, Z., Li, J., and He, C.: Spatial-temporal variations of groundwater storage in China: A multiscale analysis based on GRACE data, Resources, Conservation and Recycling, 197, 107088, https://doi.org/10.1016/j.resconrec.2023.107088, 2023.